Potential Use of Basalts from Thailand in Mineral Fibre Production

Reinhard Conradt and Preeda Pimkhaokham
Department of Materials Science,
Faculty of Science
Chulalongkorn University

1. INTRODUCTION

Among the several insulation materials applied in civil and industrial constructions, man made mineral fibres take a prominent place. Among those, alkali borosilicate glass fibres on the one side and rock, basalt, or stone fibres on the other side have the largest share. It is true, there is some overlapping in the market, however, glass and basalt fibres are complementary products rather than competitors. The weakness of one product is compensated by superior properties of the other one, and vice versa. Table 1 contrasts some key features. If compared to the alkali borosilicate fibres, basalt fibres have

- a somewhat lower insulation effect,
- a higher ability to withstand loads,
- a higher temperature stability.

When observing the extended construction activities in Thailand in both the civil and industrial branch, then it seems justified to assume a market demand for basalt fibres. There typical applications are:

- flat roof insulation (able to directly take on a bitumen paper insulation, eventually taking the weight of maintainance personal),
- fire protection (e.g., fire-proof doors in high buildings),
- heat insulation at elevated temperatures (e.g., industrial heat insulation, stack insulation, etc.),
- sound insulation of hot machine parts (e.g., motor exhaust parts).

At present, such products have to be imported, which makes them unreasonably expensive and, by this, limits their application. The lack of a local production is in contrast to the abundant occurence of basalt formations in Thailand. This has been demonstrated in an extended geological study which includes more than 25 occurrences in the Central, Northern, and North-Eastern part of the country [1]. It is the intent of the present paper to survey these local basalt occurrences from the point of view of a materials scientist, i.e., with respect to a potential utilization in mineral fibre production.

2. MATERIALS

2.1. Pre-requisites for mineral fibre production

Not every basalt is suited as a raw material for mineral fibre production. A suited material has to meet a rigid profile of requirements. This profile can be directly derived from the individual steps of the melting and fibrization process. Actually, there are several quite different processes. However, they all require raw materials with more or less the same specification. In the present paper, the commonly used tank melting and steam blowing process may serve as an example. In this process, basalt fractions of 5–20 mm are molten in a conventional glass melting tank,

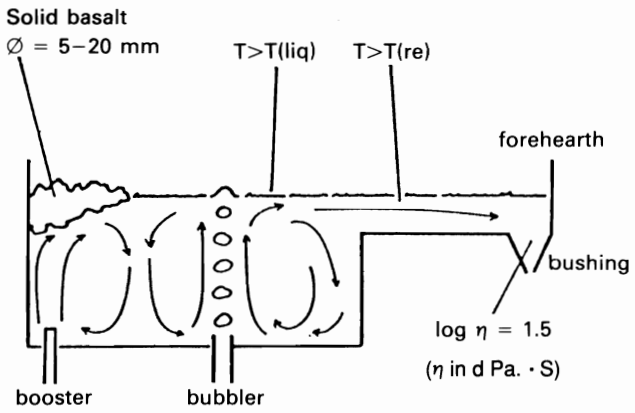

Fig. 1. Illustration of a tank melting and steam blowing process for basalt fibre production

Table 1. Comparison of typical properties of a basalt wool and a borosilicate fibre glass material

property	basalt	glass
fibre diameter in μm	6–14	4–6
density in kg/m^3	130	30
stability against loads	high	low
heat conductivity in W/(m·K)	0.045	0.035
relative insulation effect	1	1.5
pull viscosity in dPa·s	30	1000
pull temperature in °C	1360	1060
max. application temperature in °C	700	450

processed into fibres by a steam jet of approx. 10 bar, coated with a binder or a resin, collected, heat treated, cut into mats or other shapes, and packed. For high-temperature applications, the binder or resin is omitted, and the mats are chattered by metal wires instead. The core piece of the process is the so-called bushing block, i.e., a refractory block at the end of the forehearth equipped with a V-shaped platinum sink. This sink, called bushing, has about 50 holes (tips) in its bottom. The adjustment to the appropriate pull temperature is established in the bushing by direct electrical heating. The melt flows from the bushing tips, is accelerated by the expanding steam jet, and pulled into an irregular sequence of individual fibres. Details on the process may be taken from [2], [3]. The sketch in figure 1 illustrates some of the implications of the described process. They are presented below in terms of a profile of requirements:

- The most important criterion is set by the temperature T(1.5) at which the melt assumes a viscosity of $10^{1.5}$ or 30 dPa·s. This is the viscosity at which a basalt melt can be processed into fibres, the so-called

log η = 1.5 level. For established production lines, T(1.5) values of 1340 to 1385°C are reported [4]. This may give an impression of the permissible range for T(1.5).

- Re-crystallization in the bushing or in the forehearth would inevitably clog the bushing tips. Therefore, the upper temperature of re-crystallization T(re) of the basalt melt must be significantly lower than T(1.5), and also lower than the forehearth temperature.
- Re-crystallization problems are even enhanced when high-liquidus inclusions in the basalt are not completely dissolved during the melting process. Therefore the temperature of complete melting, i.e., the thermodynamic liquidus temperature T(liq) must not exceed the available process temperature.
- The electrical resistivity r of the melt must allow electric heating at two different temperature levels. Electrical heating is required, not only in the bushing but also in the batch melting region. In contrast to a conventional glass batch, which is able to float on top of the melt, a basalt tends to sink down to the cooler bottom of the tank. If this were allowed to happen, no satisfactory melting would be possible. As a counter-measure, a strong local convective up-stream has to be generated in the melt by electrical boosting, able to keep basalt fractions < 20 mm afloat.
- The basalt must melt down fast enough so as to allow an economic throughput of melt. Therefore information is needed on the kinetics of macroscopic fusion, i.e., on the temperature T(fuse) where the majority of the basalt matrix melts, and on the time consumed for fusion.

2.2 Predictive models

Predictive models in glass technology are an important tool to minimize the amount of (expensive) experimental work. Based on an evaluation of previous experimental work, they allow to derive reliable estimates of material properties from the chemical composition. In the present case, such models had to be used to perform a pre-selection among the numerous raw materials already surveyed in [1], so as to reject the unsuited ones right from the start. Furthermore, the models were used to cross-check the accuracy of experimental results.

A very simple yet widely accepted "model" makes use of the so-called acid modulus S and basic modulus B defined by

(1 a) $S = (SiO_2 + Al_2O_3) / (CaO + MgO)$,

(1 b) $B = (100 - SiO_2 - Al_2O_3) / (SiO_2 + Al_2O_3)$

The respective oxide amounts have to be inserted as wt. %. For a basalt fibre process, $2.5 < S < 3.0$ and $0.65 < B < 0.75$ are used as a common guideline. As basalts from Thailand are comparably rich in alkali (not taken into account by S and B), the criterion may be too restrictive.

A more elaborated model including all oxide components was developed by Zagar and Schaefer-Rolffs [4]. It makes use of the Vogel-Fulcher equation

(2) $\ln \eta = 2.303 \cdot \log \eta = A + B/T$, T in K, η in dPa·s

to predict the viscosity-temperature relation of basalt melts in the high-T range, i.e., for $\log \eta < 3.0$. The constants A and B are calculated by

(3 a) $A = A(0) + \Sigma_j A(j) \cdot y(j)$,

(3 b) $B = B(0) + \Sigma_j B(j) \cdot y(j)$.

The y(j) are the weight fractions (i.e., the wt. % divided by 100) of the oxides j. The increments A(0), B(0), and A(j), B(j) are given in table 2. The average composition of basalts from Thailand fits well with the range of validity of this model.

Lakatos et al. [5] developed a model to predict the viscosity levels T(1.5), T(2.0), T(2.5), as well as the liquidus temperature T(liq) of basalt melts. Unfortunately, the range of validity of this model is not compatible with the composition range of local basalts.

Finally, experimental data on electrical resistivities [4] were evaluated and submitted to a multiple regression analysis. Temperature dependence of resistivity strictly followed the relation

(4) $r = a \cdot \exp(b/T)$,

T in K, r in Ω·cm. The regression was performed to correlate the constants a and b to the composition of the basalt melts. After some

trial and error, the following set of variables were chosen:

- the weight fraction of SiO_2,
- the sum of weight fractions of MgO and CaO
- the sum of weight fractions of alkalies,
- the molar acidity modulus S''.

Where the parameter S'' is given by

(5) $S'' = (SiO_2/60.064 + Al_2O_3/101.961) / (MgO/40.311 + CaO/56.079)$.

The resulting increments a(0), b(0) and a(j), b(j) for the two constants a and b in equation 4 are compiled in table 3. The constants a and b are calculated like in equations 3 a–b. The model reproduces the original data base between 1200 and 1450°C very well (mean deviation 2%, max. deviation 5%).

It must be stressed that, except for the S and B criterion, the presented models are based on extended data bases of experimental results, and beside this, do require further experimental results (i.e. a full chemical analysis) before they can be applied. That is why these model usually give reliable estimates of the true properties.

2.3. Sample collection

Sample collection was based on the comprehensive geological study [1], as well as on the predictive models mentioned above. Samples were collected from such sites only where a suited basalt material could be expected. The selected locations are summarized in table 4. From each basalt field, several samples from different locations were taken. BR and PPK samples were taken from established quarries; the sampling depth was in the range of 10 to 30 m. As to the other sites: Measures had to be taken to avoid surface sampling of strongly wheathered material. Therefore, such

Table 2. Factors for the calculation of the viscosity-temperature relation of basalts after equations 3 a–b

oxide j	A (j)	B (j)	oxide j	A (j)	B (j)
SiO_2	108.76	−157313	MgO	67.02	−106326
TiO_2	164.63	−298390	CaO	152.79	−251610
Al_2O_3	72.96	−93954	Na_2O	31.62	−10552
Fe_2O_3	138.45	−244990	K_2O	179.40	−299914
FeO	142.33	−248015	j = 0	−118.33	187609

Table 3. Characteristic factors for the calculation to the electrical resistivity of basalt melts in Ω·cm;
δ: absolute standard deviation of the estimate;
r^2: squared regression coefficient;

j	quantity	$10^5 \cdot a(j)$	$10^{-4} \cdot b(j)$
0	constant	5.5364	0.70988
1	SiO_2	−0.0135	0.02529
2	MgO+CaO	−0.3008	0.04076
3	alkali	0.5852	−0.13226
4	S''	−0.1403	−0.01266
	$\pm \delta$	0.2526	0.03242
	r^2	0.9928	0.9928

sampling locations were chosen where, e.g., a road cut through a hillside. By this, sampling depths in the range of 2 to 5 m could be reached. For reasons of comparison, a basalt from Germany (Westerwald), GH, was included in the study. This basalt is being used in a fibre production process and thus may serve as a reference for the applicability of other materials.

3. EXPERIMENTAL METHODS

3.1 Chemical analysis

X-ray fluorescence was chosen as the appropriate method to perform a full analysis on larger numbers of similarly composed samples. Basalt samples were molten in small fire clay crucibles (inner diameter ≈ 2.5 cm, height ≈ 4 cm) and cut into slices by a low-speed saw. The cutting blade used is designed to produce a surface of ± 3 µm roughness. So, no further polishing was required.

Pre-tests on standards with known composition were performed to determine which mode of X-ray discrimination was required for the different elements. For elements Na, K, Mg, and Fe, the fast, however less accurate *energy*–dispersive discrimination (EDX) was sufficient. The reproducibility factors for these elements, i.e., the factors by which the analytical results have to be multiplied to match the nominal element concentrations in the standard, were 1.000, 0.992, 1.033 and 1.021, respectively. By contrast, the factors for Si, Al, and Ca were 0.953, 1.356 and 0.908. For the latter elements, the EDX mode was insufficient, and the time consuming *wavelength*-dispersive discrimination (WDX) had to be applied. For the purpose, the commercial glass JM 753–C [6], the certified standard glass DGG–1 [7], and two further standards A and B, prepared as artificial basalts, were employed. Table 5 shows the contents of SiO_2, Al_2O_3, and CaO in the four standards. Table 6 shows the correlation between the analytical signals (cps = counts per second) and the elemental concentrations for selected triplets of the above standards. Self correlations (e.g., cps Si vs. wt, % SiO_2) were satisfactory. The table also reveals very strong cross correlation (e.g., cps Ca vs. wt. % Al_2O_3). This is the reason why the EDX mode failed for Si, Al, Ca. By employing the above standards, the cross correlation effects were determined quantitatively, This served, in turn, as a basis to correct the immediate WDX results.

Table 4. Overview over the locations of investigated basalts

name of location	symbol after [1]	geological map no.
Mae Tha, Lampang	MT	NE 47–7
Sop Prap, Lampang	SP	NE 47–7
Khao Kradong, Buriram	BR	ND 48–5
Phu Phra Angkhan	PPK	ND 48–5
Khao Pha Nom Rong	PR	ND 48–5
Prai Bat	BY	ND 48–5
Wichian Buri	WB	NE 47–4

3.2. Viscosity-temperature relation

Viscosity determination of an oxide melt in the high-T range is a very difficult and demanding experimental task. The commercial apparatus recommended for this task is a rotation viscosimeter with a Pt crucible and a honed Pt rotator attached to a sensitive torque gauge. Since this type of equipment was not available, a completely new method of viscosity determination was developed. This method is comparably simple, does not require any Pt

Table 5. Amounts of silica, alumina, and calcia in selected standard glasses

standard	SiO_2	Al_2O_3	CaO
JM 753–C	63.40	5.10	6.20
DGG–1	71.72	1.23	6.73
glass A	46.63	15.54	7.25
glass B	52.63	9.68	9.47

Table 6. Correlation between the cps of the elements Si, Al, and Ca by wavelength-dispersive X-ray fluorescence analysis and the respective amounts of oxides in selected combinations of standards, given in terms of the squared correlation coefficients

combination of standards	oxide	correlation of wt. % to cps Si	cps Al	cps Ca
JM 753–C; DGG–1; glass A	SiO_2	1.000	0.996	0.781
	Al_2O_3	0.994	1.000	0.834
	CaO	0.417	0.488	0.866
JM 753–C; DGG–1; glass C	SiO_2	0.999	0.995	0.593
	Al_2O_3	0.996	0.990	0.568
	CaO	0.715	0.747	0.992

equipment, and yet yields results with a remarkable precision. We may call it the outflow test.

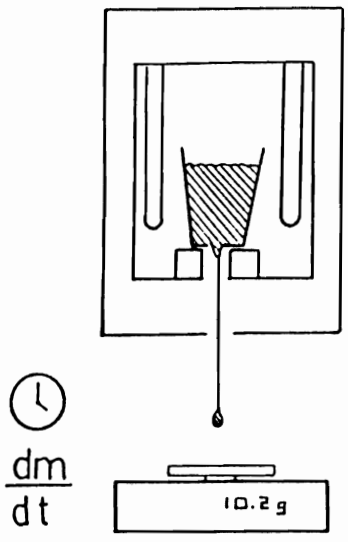

Fig. 2. Illustration of the outflow test for viscosity determination in the range lpg η = 1.0 to 3.0, η in dPa·s

The method is illustrated in figure 2. A commercial fast heating high-T furnace with a very accurate temperature control was modified, i.e., equipped with an orifice in the bottom. A balance (0.01 g resolution is sufficient) was installed right under the orifice. Small alumina-clay crucibles suited for amounts of 15 to 20 g of cullets were prepared with a 5 mm orifice in the bottom. For a viscosity measurement, a sample was weighed into the crucible, placed onto a refractory ring support in the furnace and heated to the desired temperature level. The mass of glass flowing out from the orifice of the crucible was recorded as a function of time. The viscosity of the melt was read from the slope B of the mass vs. time curve by

(6) $\log \eta = \log C - \log B$

with η in dPa·s, B in g/100 s. The calibration constant C was determined from basalt GH for which the viscosity was known. At T = 1360°C, C = 296.1 was found.

Viscosities in the low-T range were determined by dilatometry. A typical dilatogram, i.e., the relative length change as a function of temperature, is shown in figure 3. The method is usually employed to determine the thermal expansion coefficient α_T of materials. Beyond this, the glass transition temperature T_G (corresponding to log $\eta \approx 13.0$) and the dilatometric softening point T_M (corresponding to log $\eta \approx 11.3$) of a glassy material can be read from a dilatogram, too. T_G and T_M are indicators for the maximal temperature of long term application of a mineral fibre material.

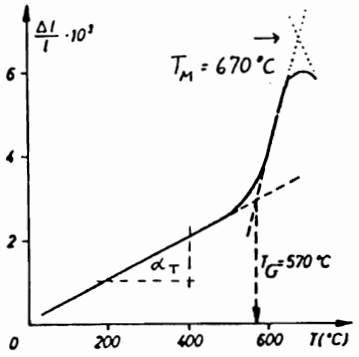

Fig. 3. Typical dilatogram of a glassy material; broken lines illustrate the determination of α_T, T_G, and T_M

3.3 Melting and crystallization kinetics

The macroscopic melting behavior was investigated in an electrically heated tube furnace (4 cm diameter, 1 m long). Basalt samples of 0.9±0.05 g were exposed to the isothermal zone in the center part of the tube, and the times t(soft), t(half), and t(fuse) to reach the softening point (where the edges of samples become round), the half sphere point (where samples assumes the shapes of a half spheres), and the point of complete fusion (see figure 4) were recorded at different temperature levels.

Differential thermal analysis (DTA) was applied to screen both the melting and

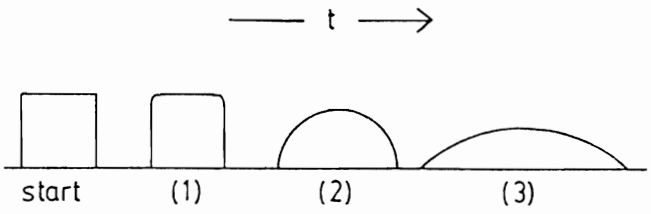

Fig. 4. Illustration of the points of round edges (1), of half sphere shape (2), and of complete fusion (3) of a sample

crystallization behavior. Samples of 150 to 200 mg were heated up to 1400°C at a rate of 10 K/min, kept there for ½ h, and then cooled down at a rate of −10 K/min. For the specific purpose of the present study, however, this method appeared to be less suited. This is because DTA primarily revealed those effects which involved major mass fractions of a sample. The effects due to the small amounts of species with the highest liquidus temperatures are easily overlooked. For the fibre production process, however, the latter species are meaningful, not the former ones. Therefore, direct observation by means of a heating stage microscope was preferred and employed as the main method. The heating stage microscope used in this study consisted of a conventional stereo microscope equipped with a special device, i.e., the so-called heating stage. The center part of the heating stage is a small alumina tube (inner diameter 1 cm) with a Pt coil which can be heated up rapidly. The upper temperature limit for the available type is 1350°C. The heating microscope can be operated in light transmission and reflection mode. A small sample < 1 mm was placed on a sample support on top of the alumina tube. The temperature was set by means of a slide regulator and read by a thermocouple. The behavior of the sample (e.g., beginning of fusion, complete melting, crystallization, etc.) was observed through the microscope. The advantage of the heating stage is its low heat capacity. So, heating and cooling cycles can be repeated frequently, and the temperatures of specific events can be approximated closer and closer. The apparatus is especially suited to determine the liquidus and re-crystallization temperatures of a substance.

4. RESULTS

4.1 Chemical composition

The corrected results of X-ray fluorescence analysis are communicated in table 7 and 8. For reasons of comparison, previous results [1] for BR, SP, and MT basalt (BR–A, SP–A, SP–B, MT–A, and MT–B), are included in the tables. The reference sample GH, together with compositions of six European basalts (B15, B19, B20, B23, B28, B30) after [4], are compiled in table 9. Fe^{2+}/Fe^{3+} ratios were adopted from [1] for the local basalt, and estimated for the European ones.

Table 7. Chemical composition of basalts from the North-East of Thailand

oxide	BR–A	BR–2	BR–3	BR–4	BR–5	PPK	PR	BY
SiO_2	48.10	50.40	50.20	49.20	51.00	52.80	51.50	51.90
TiO_2	2.40	2.70	2.70	2.90	2.56	2.50	2.90	2.80
Al_2O_3	16.50	13.20	13.00	12.80	12.99	14.30	14.50	15.00
Fe_2O_3	11.50	12.00	11.54	11.95	11.58	11.30	9.10	10.70
(Fe^{3+})	3.60	3.76	3.61	3.74	3.63	3.50	4.80	3.30
(Fe^{2+})	7.90	8.24	7.93	8.21	7.95	7.80	4.30	7.40
P_2O_5	0.78	0.57	0.57	0.67	0.63	0.67	0.95	0.70
MgO	6.40	7.15	7.20	7.90	6.80	5.20	4.70	5.40
CaO	7.10	8.50	8.40	8.60	8.30	6.70	6.40	6.80
MnO	0.12	0.20	0.20	0.24	0.23	0.10	0.11	0.11
Na_2O	3.95	3.36	4.00	3.50	3.90	4.10	4.40	3.70
K_2O	1.80	1.86	2.10	2.20	1.95	1.40	1.90	1.50

Table 8. Chemical composition of basalts from the North of Thailand

oxide	SP–A	SP–B	SP–1	SP–2	SP–3	SP–4	MT–A	MT–B	MT–0	MT–1	MT–2
SiO_2	48.20	45.50	52.44	52.74	51.67	49.30	46.50	45.90	46.40	48.94	50.30
TiO_2	2.00	2.20	2.06	2.18	2.10	2.04	2.30	2.30	2.20	2.30	2.28
Al_2O_3	17.80	17.40	16.33	16.50	16.29	15.04	15.30	18.10	13.70	14.60	15.27
Fe_2O_3	8.10	10.40	8.90	9.00	8.56	10.63	7.70	9.40	11.54	10.76	9.90
(Fe^{3+})	3.65	4.68	4.01	4.05	3.85	4.78	2.10	2.90	3.15	2.93	2.70
(Fe^{2+})	4.46	5.72	4.90	4.95	4.71	5.85	5.60	6.50	8.39	7.83	7.20
P_2O_5	0.80	0.47	0.45	0.65	0.71	0.66	0.70	0.52	0.46	0.53	0.74
MgO	4.70	6.20	5.72	5.55	5.44	7.08	7.00	6.70	9.30	8.22	6.60
CaO	7.30	8.10	7.34	7.20	7.90	8.63	9.70	7.80	9.60	8.32	8.35
MnO	0.14	0.21	0.25	0.20	0.17	0.25	0.17	0.19	0.33	0.25	0.20
Na_2O	4.40	2.80	2.80	2.51	3.20	3.10	3.80	3.40	3.80	2.90	2.70
K_2O	2.00	3.30	3.44	3.33	3.86	3.20	2.70	3.50	2.70	3.08	3.17

Table 9. Chemical composition of reference basalt GH, and of six further European basalts (B15 to B30)

oxide	GH	B15	B19	B20	B23	B28	B30
SiO_2	46.22	46.86	41.85	49.93	49.74	43.84	47.72
TiO_2	2.84	2.4	2.48	2.47	1.79	2.36	1.28
Al_2O_3	13.19	13.09	11.85	12.73	15.64	12.24	15.92
Fe_2O_3	12.50	11.28	11.15	10.22	10.68	11.69	10.41
(Fe^{3+})	3.75	5.08	5.02	4.60	4.81	5.26	4.68
(Fe^{2+})	8.75	6.20	6.13	5.62	5.87	6.43	5.73
P_2O_5	–	0.36	0.51	0.41	0.23	0.74	0.13
MgO	9.78	10.29	12.95	9.59	5.29	12.24	9.64
CaO	10.87	10.49	13.25	8.77	8.37	10.84	9.42
MnO	–	0.24	0.17	0.21	0.24	0.17	0.23
Na_2O	2.72	2.81	2.88	3.34	3.88	3.23	2.33
K_2O	1.26	1.28	0.63	1.58	0.66	1.31	0.68

An evaluation of tables 7 to 9 with respect to the acid modulus S and basic modulus B is shown in figure 5. According to this evaluation, none of the local basalts matches the criterion $2.5 < S < 3.0$ and $0.65 < B < 0.75$. Local basalts are more acid and less basic than the European ones. So we may expect less free play in the selection of suited materials. Figure 6 points to another significant difference among the basalt. Local basalts are comparably rich in both alumina and alkali. Based on this diagram, we may question the validity of the S and B criterion, since it does not take into account alkali at all.

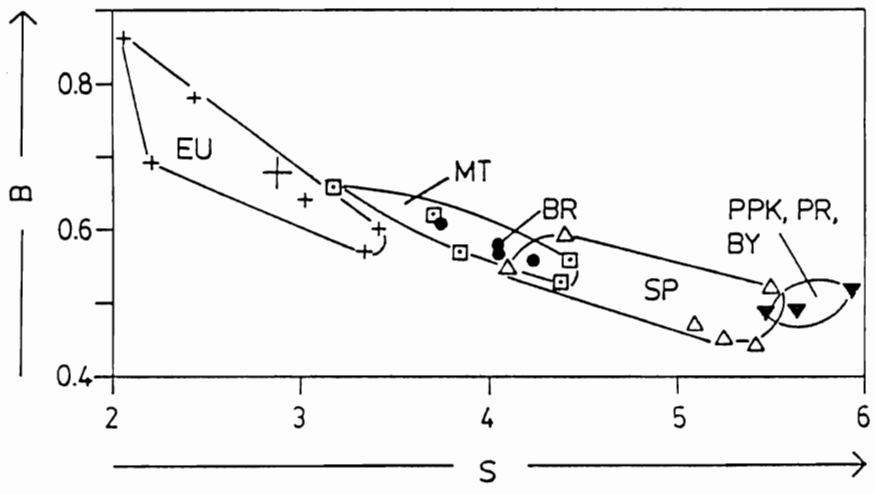

Fig. 5. Basic modulus B vs. acid modulus S plotted for local and European (EU) basalts; the large cross represents sample GH

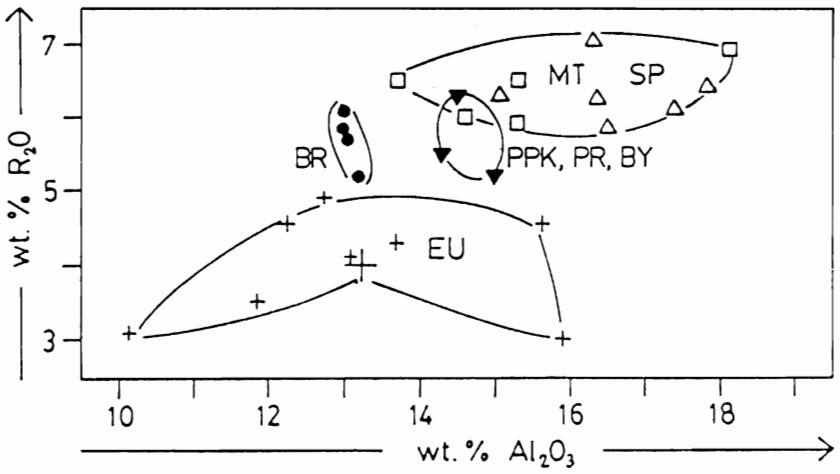

Fig. 6. Alkali oxide vs. alumina content plotted for local and European (EU) basalts; the large cross represents sample GH

In a next step, the analytical results were used to perform a CIPW calculation (named after the petrologists Cross, Iddings, Pirrson, and Washington; see [8]) for the normative mineral content of the investigated samples. In principle, this procedure corresponds to approaching the phase diagram of a multi-component system. The different mineral phases used in the calculation are summarized in table 10. When the mineral phases are grouped together as igneous minerals, feldspatic minerals, and quartz, then the pseudo-ternary phase diagram in figure 7 is obtained. Again, significant differences between the local and European basalts surface. The former ones have a comparatively low content of igneous minerals. Basalts from BR and MT come closest to the location of the reference material. It is most interesting to relate this observation to the viscosity data reported below. Indeed, BR and MT are the only species with a potential to meet the stringent viscosity criterion of a fibrization process. Anticipating this result, we may conclude that the phase diagram in figure 7 represents best the overall differences and similarities among the different basalts.

Table 10. Mineral phases use to present the normative mineral content of basalts

mineral name	stoichiometry
apatite	$3\ (3CaO{\cdot}P_2O_5) \cdot CaF_2$
ilmenite	$FeO \cdot TiO_2$
sphene	$TiO_2 \cdot CaO \cdot SiO_2$
orthoclase	$K_2O \cdot Al_2O_3 \cdot 6SiO_2$
albite	$Na_2O \cdot Al_2O_3 \cdot 6SiO_2$
nepheline	$Na_2O \cdot Al_2O_3 \cdot 2SiO_2$
anorthite	$Ca_2O \cdot Al_2O_3 \cdot 2SiO_2$
magnetite	$FeO \cdot Fe_2O_3$
hematite	Fe_2O_3
Mn silicate	$MnO \cdot SiO_2$
diopside	$CaO \cdot (Fe, Mg) \cdot 2SiO_2$
hypersthene	$(Fe, Mg)O \cdot SiO_2$
olivine	$2\ (Fe, Mg)O \cdot SiO_2$
quartz	SiO_2

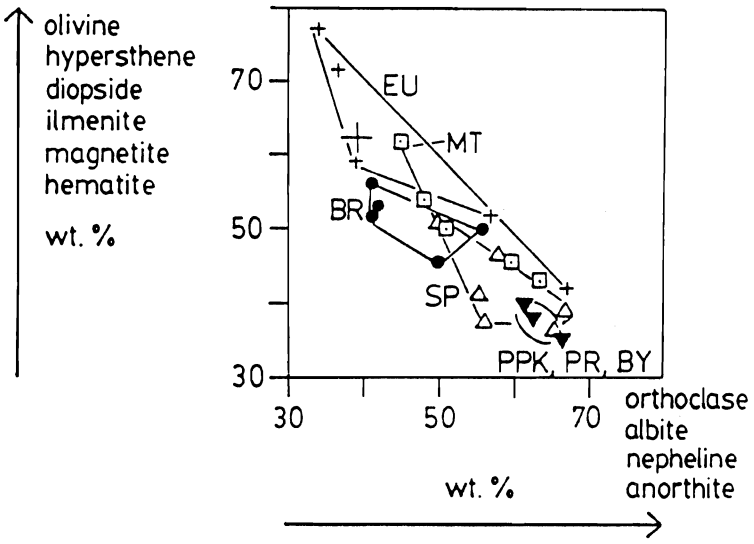

Fig. 7. Pseudo-ternary phase diagram for basalts for local and European (EU) basalts; the large cross represents sample GH; the balance to 100% is mainly due to quartz

4.2. Viscosity-temperature relation

High- and low-T viscosities were determined experimentally as described in section 3.2. In addition to this, analytical results from tables 7 to 9 were used to calculate high-T viscosities as described in section 2.2. Beyond this, the viscosity level T_L (so-called Littleton temperature; for log η = 7.6) was determined by interpolating between high- and low-T values. T_L can be interpreted as an idicator for the short term stability of a basalt fibre, e.g., in fireproof applications. The results are summarized in table 11. Especially the results for high-T viscosities are the very key for the selection of suited materials. It is stressed once again that the calculated viscosity values are not any less well based on experiments than the ones directly measured. And indeed, both data sets reflect the same tendencies. Differences may be due to experimental errors, but also to within-site scatters of the chemical composition. Anyway, the conclusions are unambiguous: Only basalts from BR and MT have viscosities low enough to be further considered as candidate materials. All other basalts investigated are far too viscous for a fibrization process. Viscosity data in the low-T range do not show any dramatic effects. For the potentially suited basalts BR and MT, they are slightly lower than for the reference material

Table 11. Glass transition temperature T_G and dilatometric softening point T_M (both by experiment), Littleton temperature T_L (by interpolation), and viscosities η in dPa·s, as determined by experiment and calculation

balsalt	T_G	T_M	T_L --- = 1360 °C ---				
				calculation		experiment	
	°C	°C	°C	log η	η	log η	η
GH[1)]	685	775	982	–	–	1.51	32
GH[2)]	–	–	–	1.40	25	–	–
BR–2	680	744	918	1.71	51	1.85	72
BR–3	635	707	899	1.77	59	1.76	57
BR–4	633	703	890	1.62	42	1.75	56
PPK	657	721	–	2.04	110	2.21	165
PR	663	741	–	2.06	114	2.46	291
BY	673	759	969	2.00	100	2.15	143
SP–1	666	723	890	2.11	129	2.25	177
SP–2	713	818	1041	2.09	124	–	–
SP–3	–	–	–	2.11	129	–	–
SP–4	703	773	954	1.82	66	–	–
MT–0	680	731	808	1.64	43	–	–
MT–1	662	716	874	1.75	56	1.96	91
MT–2	669	730	901	1.87	75	2.04	110

1) sample available for experiments
2) different sample as analysed abroad

GH. This means, these basalts are slightly less stable towards heat.

4.3 Melting and crystallization kinetics

The most meaningful parameters on melting and crystallization were determined by heating stage microscopy. These are:

T (fuse): the temperature of fusion; this is the temperature where the grains start to melt down upon slow heating-up during the first heating cycle; this temperature refers to macroscopic melting like the fusion time t(fuse) determined in the tube furnace;

T (liq): the liquidus temperature; this is the temperature where all crystalline particles completely dissolve when the temperature is increased in small steps beyond T(fuse); several heating and cooling cycles with decreasing step width were required to approximate T(liq);

T(re): the temperature of re-crystallization; this is the temperature where the first crystals start to form when the temperature is decreased stepwise below T(liq); again, several cycles were required to approximate T(re).

Table 12. Melting and re-crystallization behavior of basalts in comparison to the reference sample GH; all temperatures in °C; t is s;

basalt	T (fuse)	T (liq)	T (re)	T (max)	t (fuse) for T in °C		
					1200	1250	1300
GH	1290	1300	1240	1081	260	141	80
BR–2	1295	1315	1245	1033	227	121	67
BR–3	1300	1300	1218	1039	411	145	55
BR–4	1298	1318	1235	1031	196	120	76
SP–1	1280	>1320*)	1265	1002	179	98	56
SP–4	1295	>1300*)	1253	1005	233	141	89
PPK–1	1285	1290	1235	1019	219	129	79
PPK–2	1299	1330	1260	1011	262	149	88
PPK–3	1293	1320	1255	1008	198	137	97
PR–1	1277	1290	1228	1053	309	171	98
PR–2	1290	1300	1245	1021	276	154	90
MT–0	1280	1320	1250	971	227	112	58
MT–1	1290	>1330*)	1268	1037	228	112	58
MT–2	1280	>1320*)	1268	1039	179	104	62
BY	1330	1295	1238	995	#)	–	–
WB	–	–	–	–	@)	–	–

*) minor amounts of a crystalline phase did not dissolve during the T (liq) test

#) t (1277 °C) ≈ 220 s, t (1263 °C) ≈ 400–800 s;

@) t (1277 °C) ≈ 320–450 s

T(fuse), T(liq), and T(re) are presented in table 12. Next to the high-T viscosities, these quantities determine whether or not a basalt is suited for a fibrization process. An inspection of the fusion temperatures in table 12 shows that the potentially suited basalts BR and MT deviate from the reference sample by 10 K or less in either direction. A survey of the liquidus temperatures shows that for most materials, T(liq) does not exceed 1320°C. This is considered acceptable. By contrast, all samples from the SP field, as well as samples MT-1 and MT-2 retained minor amounts of a microscopic crystalline phase even at 1330°C. The consequences of this finding become obvious when the re-crystallization temperatures are compared. The SP, MT-1, and MT-2 basalts displayed very high re-crystallization temperatures. This is understood from the fact that the residual crystallites acted as heterogeneous nuclei during cooling, thus accelerating re-crystallization. An the other side, all BR basalts and the MT-0 basalt exhibit favourably low T(re) values. The stability of these materials towards re-crystallization is sufficient for a production process.

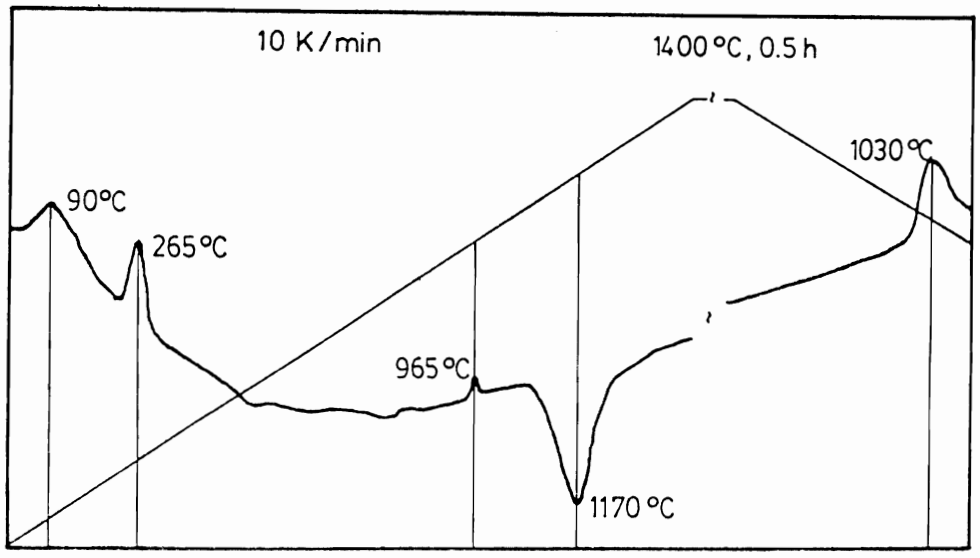

Fig. 8. DTA graph for a typical basalt sample showing the DTA signal (bold curve) and the reference temperature (fine curve) as a function of time; arbitrary units

Additional information on melting and re-crystallization was obtained by DTA. The DTA graphs of all basalt samples showed a pattern very similar to the one presented in figure 8. All basalts showed two exothermic low-T peaks, one below 100°C, one at ≈ 265°C. No interpretation can be offered for these peaks (since a release of water would yield endothermic rather than exothermic effects). A deep endothermic peak between 1000 and 1200°C indicates the melting of the bulk of crystalline material T(bulk). A strong exothermic peak occuring somewhere between 1100 and 950°C upon cooling indicates the crystallization maximum T(max). T(max) is listed in table 12. Both T(bulk) and T(max) refer to the compounds constituting the majority of the material. Neither of them necessarily refer to the crystalline species which dissolves last and appears first. Thus, in general T(bulk) is different from T(liq), and T(max) is different from T(re).

Finally, the times t(soft), t(half) and t(fuse) were determined at different temperature levels between 1180 and 1280°C. The experimental scatter in these experiments was quite high. So a total of 20 to 50 samples per basalt species

Table 13. Electrical resistivities in Ω · cm for different basalts at indicated temperatures in °C, calculated from the chemical composition

basalt	1200	1300	1400
GH	42.85	16.89	7.44
BR–2	66.41	30.61	15.48
BR–3	49.23	23.99	12.74
BR–4	50.40	24.33	12.81
BR–5	58.40	27.85	14.51
SP–1	51.05	23.19	11.58
SP–2	58.78	25.96	12.64
SP–3	35.73	17.16	8.99
SP–4	38.13	18.32	9.60
PPK *)	66.61	30.00	14.86
PR *)	39.89	19.03	9.92
MT–0	27.30	13.96	7.74
MT–1	42.28	20.15	10.49
MT–2	48.34	22.35	11.33
BY	64.40	28.42	13.83

*) identification of the sample number uncertain

were investigated. The results were submitted to a multiple regression analysis and extrapolated to 1200, 1250, and 1300°C. For the time being, only t(fuse) values are communicated; they are added to table 12. Almost all basalts from Thailand melted down easily. The BR basalts and MT-0 performed particularly well. On the other side, BY and WB basalts melted down so slowly that any further investigation on the suitability of these materials became obsolent. Indeed, for WB basalt, t(fuse) remained the only experimental result determined in this study.

4.4 Electric resistivities

In the present study, electric resistivities were not determined by experiment. However, in order to supplement the property profile of the investigated basalts, resistivities were calculated from the chemical compositions. This was accomplished by the newly developed predictive model (see equations 4 and 5, and table 3). The results are summarized in table 13 for different temperatures. Resistivities of most local basalts are somewhat higher than those of reference sample GH. The differences are not expected to cause any severe limitations to a production process.

5. CONCLUSION

Among the numerous basalt occurrences in Thailand, seven fields, were pre-selected. These are: Mae Tha and Sop Prap (both Lampang); Wichian Buri; Khao Kradong (Buriram); Phu Pra Angkhan, Khao Pha Nom Rong, Prai Bat (all three south off Buriram). From each field, a certain number of samples were collected. A sample from Germany presently used in fibre production was included in the study as a reference. The chemical composition was determined by energy– and wavelength–dispersive X-ray fluorescence analysis, and the normative mineral content was calculated. As a general finding, basalts from Thailand are more acid, less basic, richer in alkali, and less igneous than basalts from Europe.

A set of key properties were determined which allowed to conclude whether or not the pre-selected materials are suited for mineral fibre production. In the order of decreasing significance, these properties comprised: the viscosity at 1360°C, the liquidus and re-crystallization temperatures, the fusion times at different temperature levels, temperatures of maximal crystallization, low-T viscosities, and other parameters.

Most basalts from Thailand were found to be too viscous for a fibrization process. Only basalts from the Buriram and Mae Tha fields reached acceptably low viscosities. Mae Tha and also Sop Prap basalts, however, showed microscopic inclusions with liquidus temperatures above 1330°C. Only one sample from Mae Tha was free of such inclusions. Except for the samples with inclusions, all local basalts showed re-crystallization temperatures favourably lower than the reference basalt. Likewise, almost all local basalts melted down faster. Basalts from Wichian Buri and Prai Bat are an exception; they required extremely long fusion times.

To conclude: The majority of the investigated local basalts have to be dismissed as potentially suited raw materials for mineral fibre production. The conclusion is based on

high-T viscosity, liquidus temperature, and fusion time. Basalt from the Buriram field come closest to the production requirements; they would however require a somewhat higher fibrization temperature.

6. ACKNOWLEDGEMENTS

The following contributions to the success of the presented study are most gratefully acknowledged:

Expertise and advise in planning, performing, and evaluating field trips by Dr. Wisut Pisutha-Arnond, Department of Geology, Faculty of Science, Chulalongkorn University, and by Mr. Nikom Jungyusuk Geological Survey Division, Department of Mineral Resources, Ministery of Industry, both Bangkok, Thailand.

Valuable discussion, and provision of production data and reference samples by Mr. Hartmut Tiesler, G+H ISOVER Glasfaser AG, Ladenburg, Germany.

Financial support by the Metallurgy and Materials Research Institute, Chulalongkorn University, and the National Center for Metal and Materials Technology, both Bangkok, Thailand.

7. REFERENCES

1. N. Jungyusuk, T. Sirinawin: Cenozoic basalts of Thailand. Conference on Geology and Mineral Resources of Thailand, Bangkok 1983.
2. W. Giengerich and W. Trier: Glass machines. Springer Verlag, Berlin 1984.
3. Ullmann's Encyclopedia of Industrial Chemistry, Vol. A II, Fibers. VCH Verlagsgesellschaft mbH, Weinheim 1988.
4. L. Zagar and W. Schaefer-Rolffs: Investigation of magmatic rocks with respect to their utilization for stone wool production. Sprechsaal 114 (1981) 498–512.
5. T. Lakatos, L.–G. Johansson, and B. Simmingsköeld: Viscosity and liquidus temperature relation in the mineral wool part of the system SiO_2–Al_2O_3–CaO–MgO–alkalies–FeO–Fe_2O_3. Glastek. Tidskr 36, (1981) 51–55.
6. Borosilicate glass product no. JM 753–C, Johns Manville Co., U.S.A.
7. Standard glass DGG–1, The German Society of Glass Technology (Deutsche Glastechnische Gesellschaft).
8. See, e.g.:
   S.A. Morse: Basalts and phase diagrams. Springer Verlag. Berlin 1980.
   A.R. Philpotts: Principles of igneous and metamorphic petrology. Prentice Hall. New Jersey 1990.